TURBOMACHINERY & PUMP SYMPOSIA | HOUSTON, TX
DECEMBER 14-16, 2021
SHORT COURSES: DECEMBER 13, 2021

EFFECT OF REDUCED OIL FLOW RATE ON THE STATIC AND DYNAMIC PERFORMANCE OF A TILTING PAD JOURNAL BEARING RUNNING IN BOTH THE FLOODED AND EVACUATED CONDITIONS

Luis San Andrés — Mast-Childs Chair Professor
Andy Alcantar — Graduate Research Assistant
Turbomachinery Laboratory
Mike J. Walker'66 Mechanical Engineering Department, Texas A&M University
College Station, TX 77845

Luis San Andrés performs research in lubrication and rotordynamics, having produced technological advances in hydrostatic bearings for primary power cryogenic turbo pumps, squeeze film dampers for aircraft jet engines, and gas foil bearings for oil-free micro turbomachinery. Luis is a Fellow of ASME, STLE, GPPS, and a member of the Industrial Advisory Committees for the Texas A&M Turbomachinery Symposia. Dr. San Andrés has educated dozens of graduate students serving the profession. Dr. San Andrés earned a MS in ME from the University of Pittsburgh and a PhD in ME from Texas A&M University. Luis has published over 320 peer-reviewed papers in ASME *journals and major conferences, TPS and ATPS included.*

Andy Alcantar holds a B.S. degree in Mechanical Engineering from Texas A&M University (2019) and is pursuing a M.S. degree at the Turbomachinery Laboratory. Andy conducts experimental and analytical research in rotating machinery with emphasis on the measurement of performance and identification of force coefficients on tilting-pad journal bearings for turbomachinery applications.

ABSTRACT

The lecture presents measurements of the static and dynamic load performance conducted with a tilting pad journal bearing running under flooded and evacuated conditions and lubricated with flow rates ranging from a nominal rate to over flooded (150% nominal), and then to a starved flow (25% or lesser of nominal). The 102 mm diameter test bearing has four pads; and with single orifice feeds for the flooded condition and spray bar injection for the evacuated condition. The lubricant is ISO VG 46 oil supplied at 60ºC. The experiments include operation at two shaft speeds = 6 krpm and 12 krpm (= 64 m/s surface speed) and three applied specific loads = 0.345 MPa, 1.034 MPa and 2.068 MPa. The load is applied between pads (LBP). The lecture compares the measurements procured for the flooded bearing vis-à-vis those for the evacuated bearing and quantifies major similarities and differences. The first bearing configuration has single orifices for lubricant supply in-between pads, while the second bearing has spray bars for oil injection. A reduction in flow rate makes both bearings operate more eccentrically. The bearing under an evacuated condition operates at a larger eccentricity, which for the lowest flow rate (25% or so of nominal) does not align with the direction of the applied load, hence displaying a sizable attitude angle. Pad temperatures are similar for both bearing configurations though the evacuated bearing is colder by a few Celsius degrees and its oil exit temperature is much lower, in particular for the over flooded condition. Drag power losses derived from the oil exit temperatures show the bearing under an evacuated condition produces up to ~ 40% lesser power loss; the reduction is notable for operation with a flow rate 50% larger than the nominal flow. The bearings direct stiffnesses K_{xx} and K_{yy} increase with an applied load and show little dependency on shaft speed. The bearing operating as evacuated produces lower magnitude stiffnesses, 20% or so lesser, than the bearing running as flooded. Damping coefficients $C_{xx} \sim C_{yy}$ reduce in magnitude as the supplied flowrate decreases; the differences become marked between both bearing configurations as the load decreases. In particular for flow rates at 35% or lower of nominal, the bearing operating as evacuated shows rather small (though highly uncertain) damping coefficients. For

sufficiently small flow rates, operation at 6 krpm shaft speed and under the smallest load (0.345 MPa) produced subsynchronous shaft motions with a broad band spectrum (SSV hash). The bearing running evacuated produced SSV hash at flow rates equal to 30% or so of nominal, while the bearing operating as flooded demanded very low flow rates (~15% and lesser of nominal) to produce SSV hash. For both bearings, the SSV amplitude motions were rather small in amplitude.

INTRODUCTION

Common in turbomachinery, tilting pad journal bearings (TPJBs) are oil-lubricated elements that support with little drag or friction (multiple stage) centrifugal compressors, integrally geared compressors, power generation gas turbines, etc. Since over a century ago, TPJB load capacity, drag power loss and dynamic force coefficients are well documented with verifiable performance, experimental and analytical.

Presently, there is a need to push the performance of TPJBs to their limit by operating them with a reduced flow rate toward enabling low drag power losses and keeping within safe limits the temperature raises in both the bearings pads and the lubricating oil. A reduced flow decreases pumping costs and oil sump storage, and improves system energy efficiency. Note that operation with a too low flow rate in evacuated TPJBs, nearly unloaded, can produce the infamous subsynchronous shaft vibrations (SSV hash) [1]. A too low flow rate may also produce a quick raise in pad temperature that could degrade and even melt the Babbitt layer [2]. The final outcome could be a costly disaster [3].

The supplied flow rate into a bearing is surface speed dependent; the higher the rotor speed, the larger the required flow rate. Prior experimental research on TPJBs at the Turbomachinery Lab produced useful results for a myriad of TPJBs tested over a range of shaft speeds and applied loads, and including oil delivery systems [4]. Alas most experiments were conducted with a fixed flow rate, as recommended by the bearing owner. Most likely at low shaft speed, the bearings were over flooded with lubricant; whereas at a high shaft speed, the bearings likely starved of lubricant [5].

Since 2017, a research program at the Turbomachinery Laboratory aims to quantify the effects of reduced flow rate on the performance of TPJBs [6-9]. During the last two decades, the Turbomachinery Symposium published several relevant lectures that showcase the effect of reduced flow rate on bearing performance. Distinctive contributions are those of DeCamillo et al. [10, 1], Nicholas et al. [11], and Whalen et al. [12]. References [6-9] present critical reviews of the past literature, including modeling approaches and comparisons to experimental data.

At the Turbomachinery Laboratory, San Andrés et al. [6], based on Jani's thesis [7], quantify the influence of supplied oil flow rate, below and above a nominal condition (25% to 150%), on the performance of a lubricant flooded - five pad bearing with slenderness ratio L/D = 0.4, spherical pivots with pad offset = 50% and a preload ~ 0.40. The experimental conditions include operation at various shaft surface speeds (32 m/s-85 m/s) and specific unit loads (load per projected area) from 170 kPa to 2,100 kPa. The measured drag power and the lubricant temperature rise depend mainly on shaft speed rather than on applied load. A reduction in oil flow rate to 50% of its nominal magnitude causes a modest increase in journal eccentricity, a 15% reduction in drag power loss, a moderate raise (6ºC) in pads' subsurface temperatures, a slight increase (up to 6%) in the direct stiffnesses, and a decrease (up to 7%) in direct damping coefficients. Conversely, a 50% increase in oil flow rate produces a slight increase (up to 9%) in drag power loss, a moderate reduction of pads' temperatures (up to 3°C), a maximum 5% reduction in direct stiffnesses, and a maximum 10% increase in direct damping. Importantly enough, the authors note that the bearing drag power loss (P), derived from a direct measurement of the drive torque (T_o) x shaft angular speed (Ω), differs from a conventional power estimate (P_{est}) based on the product of the supplied flow rate (Q), the lubricant density and specific heat (ρ, c_P), and the oil exit temperature rise (T_{out} - T_{in}). The appropriate location for the measurement of the oil exit temperature (T_{out}) is most important to correctly estimate the power loss.

San Andrés et al. [8], based on the work of Toner [9], report measurements conducted with a floeded TPJB lubricated through single orifices with an ISO VG 46 oil supplied at 60ºC, and with flowrate ranging from 150% to just ~5% of a nominal supply condition. The test bearing has four-pads with center pivot, its diameter D=102 mm and its length L=0.6 D. The bearing has single orifice feeds between adjacent pads. The tests include operation at two shaft speeds = 6 krpm and 12 krpm (= 64 m/s surface speed) and under three applied specific loads = 0.345 MPa, 1.03 MPa and 2.07 MPa. The measurements show the bearing drag power loss decreases by nearly 20% when the flow rate drops to 50% of nominal. However, halving the flow produces a raise in pad subsurface temperatures, ~7°C increase, for operation at 12 krpm. Flow reduction below 50% does result in even more substantial power savings; however, it also produces too hot pad temperatures that approach the safe limit for Babbitt material at 130ºC. The bearing static eccentricity (e) and direct stiffness coefficients ($K_{xx} < K_{yy}$) do not show a significant dependency of the supplied flow rate, low or high. Damping coefficients ($C_{xx} \sim C_{yy}$) decrease by ~30% as the flow rate dwindles to just a few percent of nominal flow. A test with a very low flow rate, ~ 2% of nominal, and under a light load produced the emergence of a broadband subsynchronous vibration frequency, albeit with amplitude much lower than the motion synchronous with shaft speed.

This lecture continues to quantify the effect of varying lubricant flowrate on the performance of the same TPJB described in Refs. [8,9] but configured as evacuated and with the inlet flow lubrication through spray bars. The test conditions are identical as per shaft speed (6 krpm and 12 krpm), three applied unit loads, $W/(LD)$ =345 kPa, 1.034 MPa and 2.068 MPa, and under a load between pad

configuration (LBP). In the tests, the supplied oil flowrate ranges from 150% to 25% of a nominal flow. The following shows the test data for both bearing configurations, evacuated vs. flooded [8,9], for ready assessment of their similarities and differences.

TEST RIG AND TEST BEARING DESCRIPTION

The test rig is operational at the Turbomachinery Laboratory since well over a decade [13]. References [7,9] fully describe the bearing test rig depicted in Figure 1. Jani [7] also details the test rig features and operating procedures. An air turbine drives a thick rigid rotor supported on ball bearings housed on solid steel pedestals. A split-parts bearing stator carries the test bearing, both installed in the middle section between the pedestals. A hydraulic system supplies ISO VG 46 oil to the test bearing at a constant inlet temperature T_{in}= 60°C +/- 0.5°C, and a turbine type flow meter measures the lubricant volumetric flowrate supplied. Long rods (pitch stabilizers) with very low stiffness, hold the bearing stator assembly which includes ports for oil exit, as well as instrumentation for measurement of acceleration and displacements relative to the rotor along two orthogonal directions (X, Y). A wireless, strain gauge torque meter connects the motor to the coupling and shaft and is a direct means to measure the bearing drag power losses.

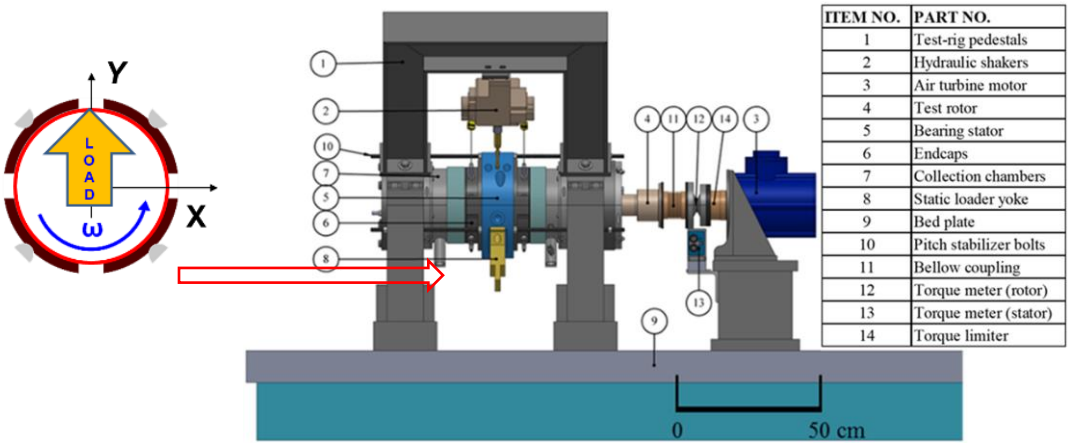

ITEM NO.	PART NO.
1	Test-rig pedestals
2	Hydraulic shakers
3	Air turbine motor
4	Test rotor
5	Bearing stator
6	Endcaps
7	Collection chambers
8	Static loader yoke
9	Bed plate
10	Pitch stabilizer bolts
11	Bellow coupling
12	Torque meter (rotor)
13	Torque meter (stator)
14	Torque limiter

Figure 1: Side view of test rig and list of major components.

The test bearing is a four-pad TPJB, 102 mm nominal shaft diameter, assembled in a load between pad configuration (LBP). The bearing is identical in geometry and configuration to the one described by Coghlan [4]. Table 1 lists the bearing geometry and materials, and Figure 2(a) displays photographs of the stator holding the bearing, the flooded bearing with one bottom half end seal removed, and a close up of the bar holding a single oil feed orifice. Similarly, Figure 2(b) depicts the evacuated bearing with oil supply through spray bars and with separate plates retaining each of the pads.

Figure 3 shows an unwrapped view of the bearing pads and thermocouples disposition. Loaded pads #1 and #2 have thermocouples embedded at their leading edge, trailing edge, and at the 75% pad arc position. In addition, thermocouples attached to the pad sides, at the leading and trailing edges of pads #1 and #2, record the lubricant inlet and exit temperatures.

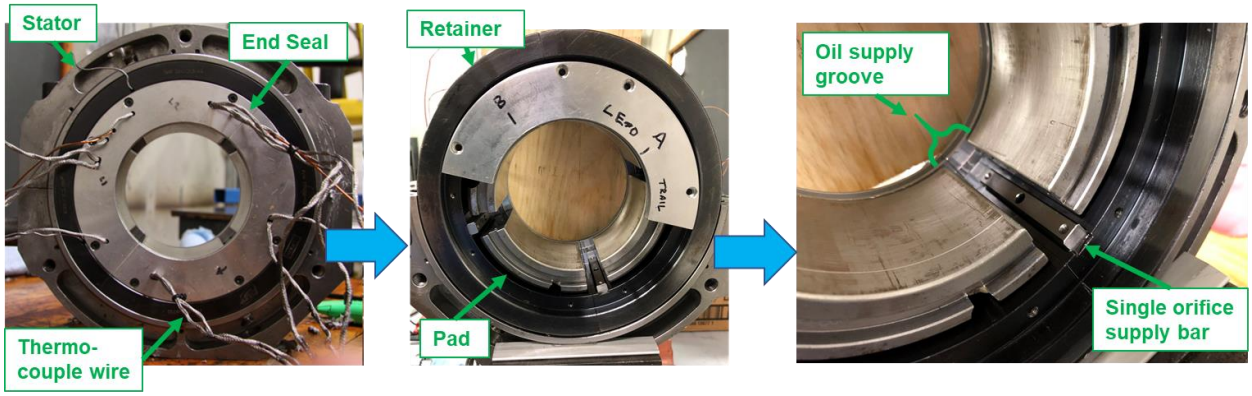

Figure 2(a): Photographs showing (a) assembled flooded bearing, (b) flooded bearing with lower half-end seal removed to reveal pads and supply groove, and (c) close up view of groove with single orifice in supply bar. Wires denote thermocouples [9].

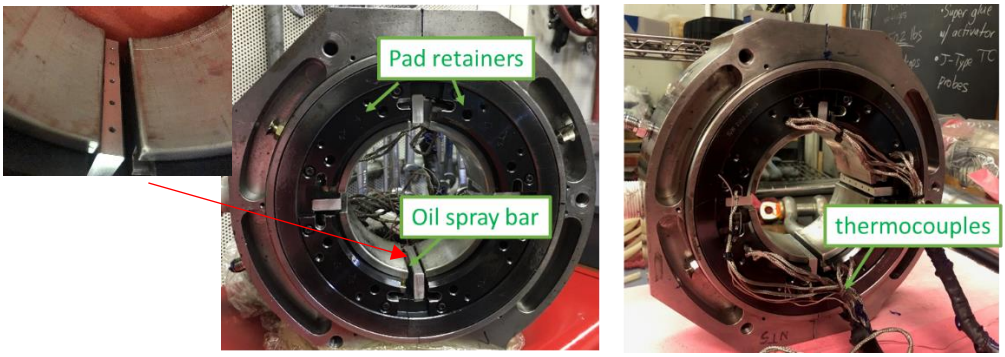

Figure 2(b): Photographs showing front and back of evacuated bearing with spray bars for oil supply.

Table 1: Four pad TPJB geometry and materials

Diameter, D	101.77 mm
Length, L	61 mm
Pivot Type	Spherical
Pivot Offset	0.50
Pad Arc Length	72°
Pad Thickness & Mass	19 mm, 0.635 kg
Pad Clearance	C_p=134 μm = C_r (1+r)
Pad Mean Preload, r	r = 0.30
Bearing Radial Clearance (Design)	C_{r*} = 103 μm +/- 7 μm.
— Cold (Room Temperature)	C_{rc} =115 μm measured
— Hot (After Test at 12 krpm)	C_{rh} = 106 μm measured
Pad Material	AISI 1018 Steel - Babbitted
Lubrication Condition	
a) Housing Type	**Flooded** (end seals with clearance 0.165 mm)
Single Orifice Size	4.4 mm diameter
b) Housing type	**Evacuated** (partial end plates guide pads)
Spray bar (edge 5 mm from pad edge)	Five orifices, diameter =5/64 inch
Lubricant Type	ISO VG 46
Supply Temperature, T_S	60°C
Viscosity (μ) at T_S	16.43 cPoise
Density (ρ) at T_S	838 kg/m^3
Specific heat (c_P)	2.08 kJ/(kg °C)
Viscosity- temperature Coefficient	0.0369 1/°C

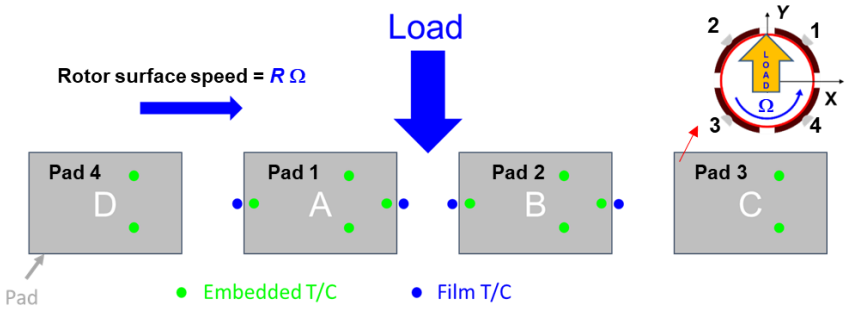

Figure 3. Schematic view of pads and location of thermocouples embedded in pads [8].

EXPERIMENTAL PROCEDURE

The goal of the experimental work is the quantification of performance of the test bearing to significant variations in the lubricant flow rate, from 150% of a nominal condition to 25% (or less). The bearing, flooded or evacuated, operates at two shaft speeds (Ω = 6 and 12 krpm) and under increasing static loads (W). Table 2 details the test conditions including the specific applied load, $W/(LD)$, i.e. load over projected area.

The nominal flow rate (Q) fully lubricating[1] all the bearing pads is easily derived as

$$Q = N_p \, ½ \, \Omega \, (½ \, D) \, L \, C_{rh} \, (1-\lambda) \tag{1}$$

where Ω is the shaft angular speed and λ~0.50 is the fraction of lubricant carried from an upstream pad. Jani [7] and Toner [9] detail the method to estimate the empirical λ. Eq. (1) is derived for bearing operation with a centered shaft (e=0), i.e., without an applied external load; hence all pads receive the same amount of lubricant (Q/N_p). At e=0, the oil flow rate that fills the gap (C_{rh}) equals to the flow area (L x C_{rh}) times the mean circumferential velocity of the lubricant (½ Ω x ½ D), i.e., 50% of the shaft surface speed.

Figure 4 displays the flow rate vs. rotor surface speed and notes the nominal condition as 100%. The results shown are derived using the bearing *hot* clearance C_{rh}=106 µm. The estimated (nominal 100%) flow rate at a speed of 12 krpm (64 m/s surface speed) coincides with the bearing manufacturer recommendation, as stated by Coghlan [4].

Table 2: Operating Conditions for tests with test bearing [8,9].

Rotor speed	Oil flow rate	Change in flow	Unit specific load, *W/(LD)*
6 krpm (32 m/s surface speed)	14.4 LPM (100%)	150% (21.6 LPM) → 25% (3.6 LPM)	0.345, 1.03 & 2.07 MPa
12 krpm (64 m/s surface speed)	28.8 LPM (100%)	150% (43.2 LPM) → 25% (7.2 LPM)	0.345, 1.03 & 2.07 MPa

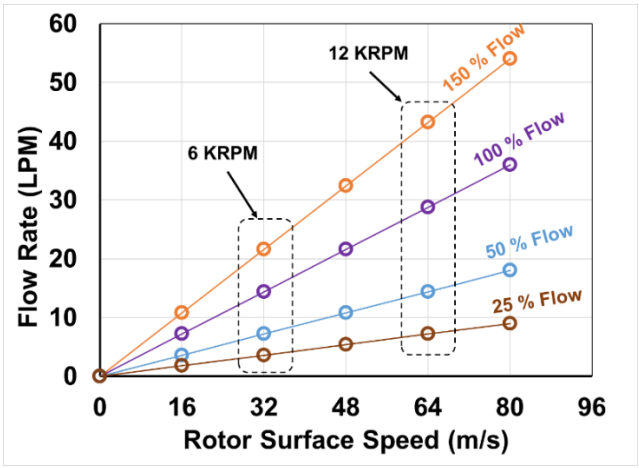

Figure 4: Lubricant flow rate vs. rotor surface speed. Same flow for evacuated and flooded bearings. Note nominal condition (100%) and changes. Used λ~0.5 and C_{rh}=0.106 mm [8,9].

A prior paper [8] and thesis [9] discuss the measurements for the flooded bearing and single orifice oil injection. Presently, experimental results for the evacuated bearing follow along with direct comparisons to those in Ref. [8]. Note the evacuated bearing configuration exchanges the single orifice oil inlet for sprays bars; see Fig. 2b. Hence, since the bearing cannot keep lubricant (accumulated) within its housing, changes in the supplied flow rate do not reach as low a magnitude as with the flooded bearing. Safety and a desire to maintain the physical integrity of the test system dictated the lowest flow rate supplied.

ESTIMATION OF THE BEARING DYNAMIC FORCE COEFFICIENTS

A two degree of freedom (X, Y) lumped parameter system represents the fluid film bearing having stiffness (K), damping (C) and added mass (M) coefficients. San Andrés [14] details the dynamic load measurement procedure along with the identification process carried in the frequency domain.

[1] The flow rate at the leading edge of bearing pad equals to the supplied flow rate plus a fraction (λ) of the flow rate leaving the trailing edge of the upstream pad, $Q_{leading\ edge} = Q + \lambda \, Q_{trailing\ edge}$.

The excitation force is built with multiple frequencies (ω) and written as $\mathbf{F}= \underline{\mathbf{F}}\, e^{i\omega t}$ where t is time and i is the imaginary complex unit. Since the test system is regarded as linear, the bearing housing acceleration $\mathbf{a}= \underline{\mathbf{a}}\, e^{i\omega t}$ and displacements relative to the spinning shaft $\mathbf{x}= \underline{\mathbf{x}}\, e^{i\omega t}$; i.e. the motion has the same frequency as the excitation.

The equation of motion in the frequency domain for the (floating) bearing with mass M_H is

$$M_H\, \underline{\mathbf{a}} = \underline{\mathbf{F}} - \underline{\mathbf{F}}_{\mathbf{B}} - \underline{\mathbf{F}}_{\mathbf{S}} \tag{2}$$

where $\underline{\mathbf{F}}_{\mathbf{S}}= (K_S\, \underline{\mathbf{x}})$ is the elastic reaction force from the soft support structure with stiffness K_S, and $\underline{\mathbf{F}}_{\mathbf{B}(\omega)}$ is the reaction force the fluid film bearing quantifies. Eq (2) is recast as

$$[\, \underline{\mathbf{F}} - M_H\, \underline{\mathbf{a}} - K_S\, \underline{\mathbf{x}}\,] \rightarrow \mathbf{H}_{(\omega)}\ \underline{\mathbf{x}} = \underline{\mathbf{F}}_{\mathbf{B}(\omega)} \tag{3}$$

where $\mathbf{H}_{(\omega)}$ is a 2x2 matrix of complex stiffness coefficients. Two independent excitation forces $[\underline{\mathbf{F}}_1 \mid \underline{\mathbf{F}}_2] = \underline{\mathbf{F}}_{12}$ with frequency (ω), produce bearing displacements $[\underline{\mathbf{x}}_{1(\omega)} \mid \underline{\mathbf{x}}_{2(\omega)}] \rightarrow \underline{\mathbf{x}}_{12}$ and accelerations $[\underline{\mathbf{a}}_{1(\omega)} \mid \underline{\mathbf{a}}_{2(\omega)}] \rightarrow \underline{\mathbf{a}}_{12}$. Then, the components of the complex matrix $\mathbf{H}_{(\omega)}=[H_{xx}, H_{xy} \mid H_{yx}, H_{yy}]$ are obtained from

$$\mathbf{H}_{(\omega)} = \underline{\mathbf{F}}_{\mathbf{B}12(\omega)}\ \underline{\mathbf{x}}_{12}^{-1} \tag{4}$$

from measurements conducted with loads spanning a discrete set of frequencies (ω).

Whenever appropriate the bearing dynamic response can be characterized with stiffness (K), damping (C) , and virtual mass (M) coefficients as $\mathbf{F_B} = \mathbf{K}\,\mathbf{x} + \mathbf{C}\, d\mathbf{x}/dt + \mathbf{M}\, d\mathbf{x}^2/dt^2$. These force coefficients are determined from curve fits of the real and imaginary components of $\mathbf{H}$, i.e.,

$$\mathrm{Re}(\mathbf{H}) \rightarrow [\, \mathbf{K} - \omega^2\, \mathbf{M}\,], \quad \mathrm{Ima}(\mathbf{H}) \rightarrow (\mathbf{C}\,\omega) \tag{5}$$

The (K, C, M) are representative of the measured data acquired over a certain frequency range, typically including $\omega = \Omega$ (synchronous shaft speed).

EXPERIMENTAL RESULTS AND DISCUSSION

The measurements with the flooded bearing happened first, as detailed in Refs. [8,9]. After, the bearing was removed and the rig reconfigured to conduct experiments with a porous surface air bearing. A year later, the original tilting pad journal bearing was installed in the test rig, spray bars replaced the original single orifice bars, and pad retainers replaced the ends seals; see Fig. 2(bottom). The second configuration is an evacuated bearing. Note that no verification of performance for the original flooded configuration took place after reinstalling the bearing in the test rig.

For the operating conditions listed in Table 2, static load characteristics measured include the journal eccentricity, pad subsurface temperatures and oil exit temperatures. Next, sets of dynamic loads excited the test bearing over a range of frequencies and the measured applied forces, bearing displacements and accelerations were used to estimate the bearing complex stiffnesses (**H**); and from these, the force coefficients (K, C, M).

Find below the results and discussion of the measurements conducted with the two bearing configurations, flooded ends and evacuated ends, as the flow rate varied from a magnitude well above nominal flow (100%) to low magnitudes, a fraction of the nominal flow rate for each shaft speed condition. Do keep in mind that the lubricant injection form for each bearing differs; the flooded bearing is supplied through single orifices, while the evacuated bearing has spray bars that shoot lubricant near the rotor spinning surface.

Bearing eccentricity

Figures 5 and 6 depict the bearing eccentricity (e) and the locus of bearing center (e_y vs. e_x) versus flow rate. Note that the eccentricity shown is relative to the *hot* center identified without any imposed load. In each figure, graphs on the left and right correspond to measurements obtained for the flooded bearing and the evacuated bearing, respectively; and while operating at a shaft speed of 6 krpm (top graphs) and 12 krpm (bottom graphs). Note the horizontal scale in the graphs of Figure 5 is logarithmic. Each graph also notes with a dashed vertical line the magnitude of the nominal (100%) flow rate at the operating speed.

The measurements show, as expected, a reduction in eccentricity (e) as the shaft speed doubles from 6 krpm to 12 krpm. A reduction in flow rate produces an increase in eccentricity, hence a lesser minimum film thickness $h_{min} \sim (C_r - e)$. For operation at 6 krpm, as the flow rate decreased from 100% nominal to 50% (7.1 LPM), the flooded bearing appears to show a sharp increase in eccentricity at a

load of 1,034 kPa, whereas the evacuated bearing shows an unexpected *jump* in eccentricity for operation under a light load of 345 kPa and with a flow rate just below 50% nominal.

For operation at 12 krpm, the evacuated bearing operates with a (modestly) larger eccentricity than the flooded bearing, in particular at the highest applied load. This behavior, however, is distinct for operation at 6 krpm which produced similar eccentricities, in particular for specific loads of 1,034 kPa and larger. The operating condition with the lowest unit load (345 kPa) shows a peculiar large increase in eccentricity as the flow reduced to 50% and below the nominal flow condition.

Recall the applied static load on the bearing is along the *Y*-direction (LBP). Thus, as shown in Figure 6, the bearing center displaces (e) parallel to the load direction, i.e., $e_x << e_y$. With the flooded bearing, the eccentricity (e) exceeds the cold clearance (C_{rc}= 0.115 mm) for operation at 6 krpm and specific load of 2.07 MPa. On the other hand, the evacuated bearing shows an eccentricity that exceeds C_r for operation at both 6 krpm and 12 krpm and under a 2.07 MPa load. A reduction in flow rate supplied to the evacuated bearing produces a significant growth in eccentricity (e), in particular for the lowest load (345 kPa).

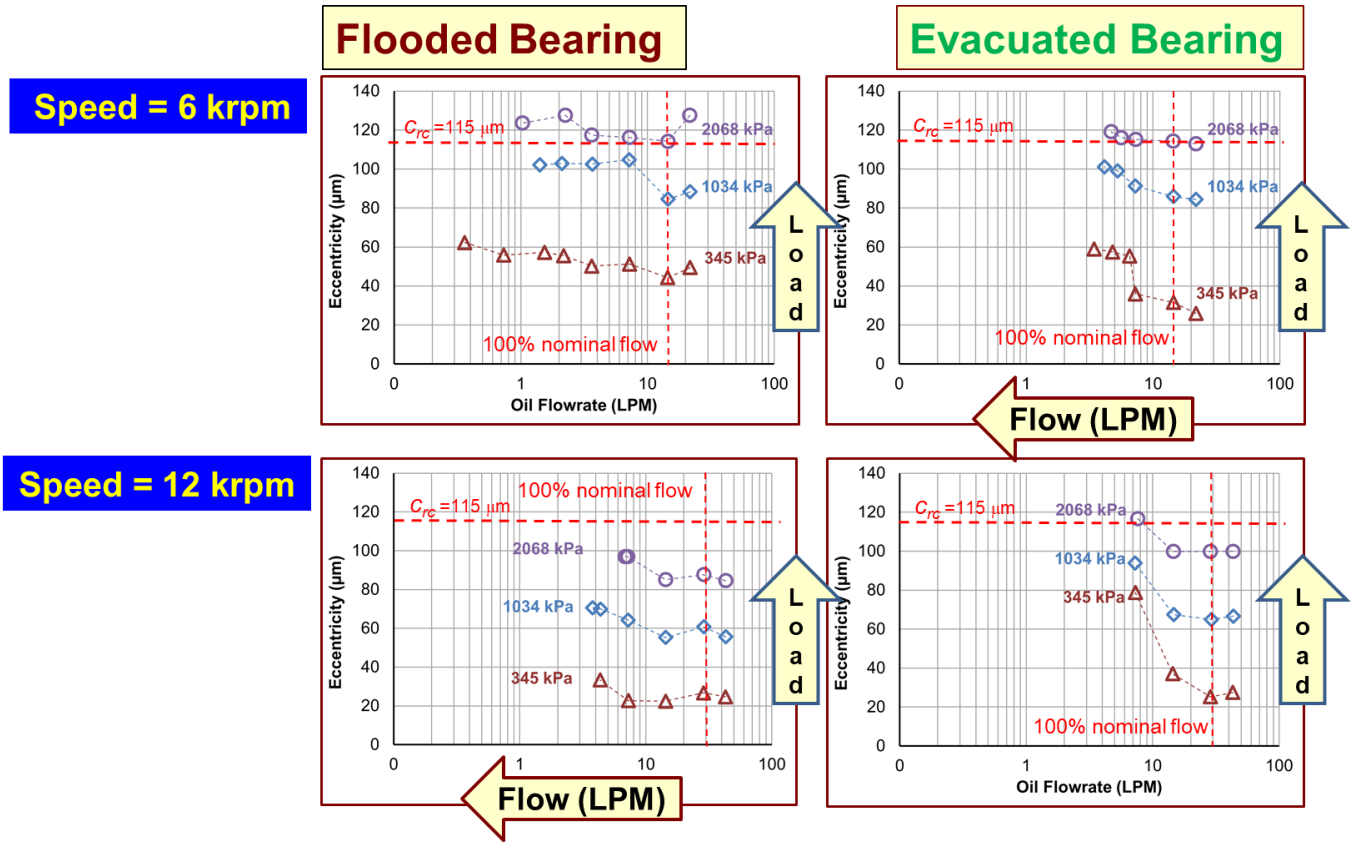

(a) Flooded bearing (orifice injection) **(b) Evacuated bearing** (spray bar injection)

Figure 5: Eccentricity (*e*) vs. supply flow rate (*Q*) for flooded bearing (left) **and evacuated bearing** (right)**. Operation with shaft speed = 6 krpm** (top graphs) **and 12 krpm** (bottom graphs)**, and three specific loads, W/(*LD*)=345 kPa, 1,034 kPa, and 2,068 kPa.**

Incidentally, note in Figure 6 that the bearing center displaces laterally as the flow rate (Q) decreases, in particular for the measurements collected with shaft speed = 12 krpm. For the lowest unit load of 345 kPa, the attitude angle is sizeable (~ 45°) albeit the uncertainty of the measurement is rather large at the lowest supplied flow rate (4.3 LPM). For the larger loads, 1,034 kPa and 2,068 kPa, the attitude angle remains small, ~10° or so, thus denoting negligible cross-coupled effects. For the evacuated bearing operating under 345 kPa unit load and 12 krpm, do note a significant lateral displacement of the shaft center as the flow rate decreases to 7.3 LPM, 25% of nominal. At this load and flow condition, it is rather unusual to report the bearing eccentricity for shaft speed of 6 krpm is smaller than that for operation at a higher speed (12 krpm).

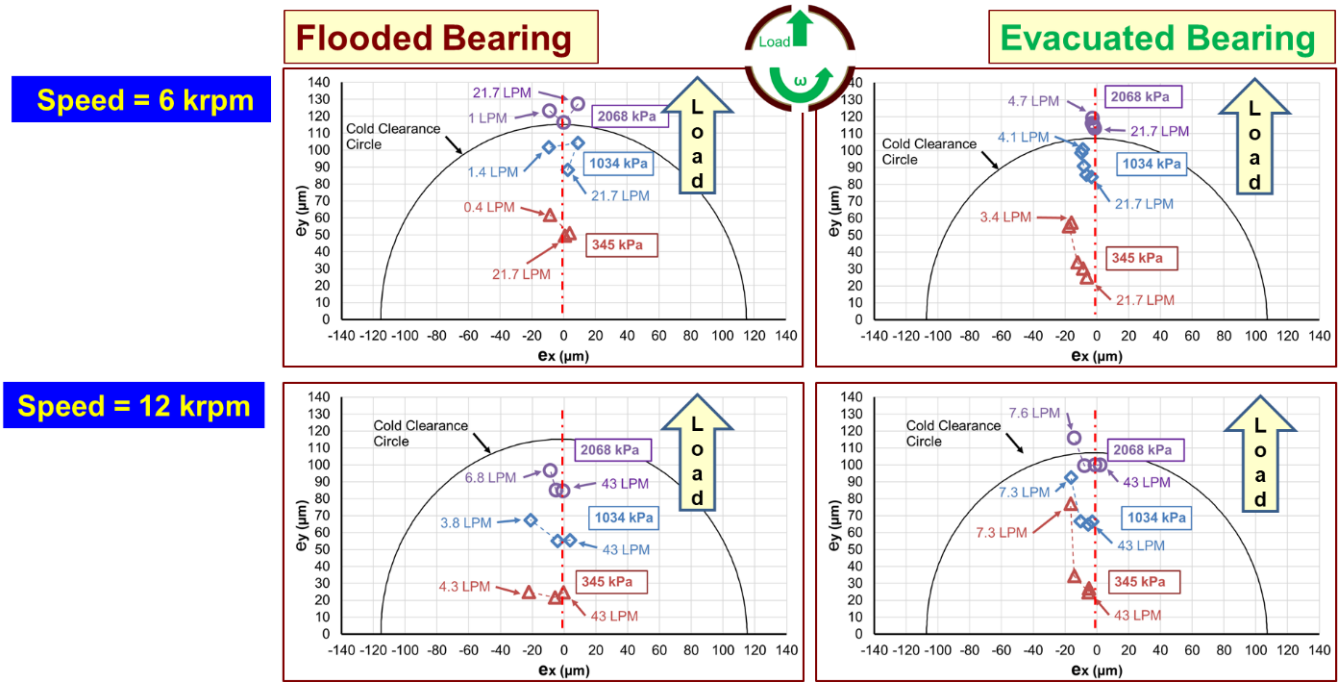

(a) Flooded bearing (orifice injection) **(b) Evacuated bearing** (spray bar injection)

Figure 6: Locus of bearing center (e_y vs. e_x) for flooded bearing (left) **and evacuated bearing** (right)**. Operation with shaft speed = 6 krpm** (top graphs) **and 12 krpm** (bottom graphs)**, and three specific loads, W/(*LD*)=345 kPa, 1,034 kPa, and 2,068 kPa. Tests conducted with various supply flow rates, high to low as noted in graphs.**

Pads' subsurface temperatures

Figure 7 depicts highest temperature rise ($\Delta T=T-T_{in}$) for loaded pad (#2) vs. flow rate for the two bearings, flooded and evacuated, and operation at 6 krpm (top graphs) and 12 krpm (bottom graphs). Figure 8 presents the highest temperature rise $\Delta T=(T-T_{in})$ vs. flow rate for the unloaded pads. Refer to Figure 3 for a layout of the thermocouples location in the pads and recall the ISO VG 46 oil inlet temperature T_{in} ~60ºC. Note the nominal flow rates for operation with shaft speed = 6 and 12 krpm equal 14.4 LPM and 28.8 LPM, respectively. Whether evacuated or flooded, the same flow rate is supplied to the bearings.

The pads' temperature increases with both shaft speed and unit load. The pad temperature also grows with a reduction in flow rate. Note that the measurements for the flooded bearing were procured with very small flow rates (5% of nominal), much lower than those supplied to the evacuated bearing[2]; and consequently, the pads in the flooded bearing show higher pad temperatures. For example, for a nominal flow condition (100%) and at 12 krpm, the evacuated bearing shows its pads are cooler (up to 5º C) than when the bearing is flooded.

For the flooded bearing, note that low flow rates (< 5 LPM), a fraction of the nominal condition, produce pad temperature rises in excess of 50ºC. Hence, the actual pad temperature is near the maximum allowable for a recommended safe operation of the Babbitt material (~ 130ºC) [2].

Note the temperature of the unloaded pads, shown in Fig. 8, displays little dependency on the specific load and does increase with shaft speed for all flow conditions. For the flooded bearing, do notice the sharp increase in pad temperature for the lowest supplied flow conditions, a fraction of 5% or so of the nominal flow. Under extreme flow starvation, the unloaded pads are just a few degrees below the peak temperature of the loaded pads, as depicted in Fig. 7.

Toner [9] presents temperatures measured on the internal feed groove that routes the lubricant to the orifices between the bearing pads. This groove locates on the outer diameter of the bearing cartridge. For most flow conditions (high or low), the temperatures recorded equal T_{in} ~ 60ºC, the specified oil inlet temperature. However, with the flooded bearing and for very low flow rates (5% or less of nominal), the groove temperatures increase sharply on the loaded side of the bearing and are not steady. The large temperature difference likely induced a mechanical deformation of the bearing. Similar results are not available for the evacuated bearing as the flow rate supplied did not reach such low magnitudes. That is, for the data hereby reported, the bearing OD and oil feed groove maintained their temperatures at a magnitude close to the oil inlet temperature, T_{in} = 60ºC.

[2] Operational safety and test element integrity dictated the lowest flow rate with the evacuated bearing since there was no certainty on whether one or more pads had reached concerning levels of oil starvation.

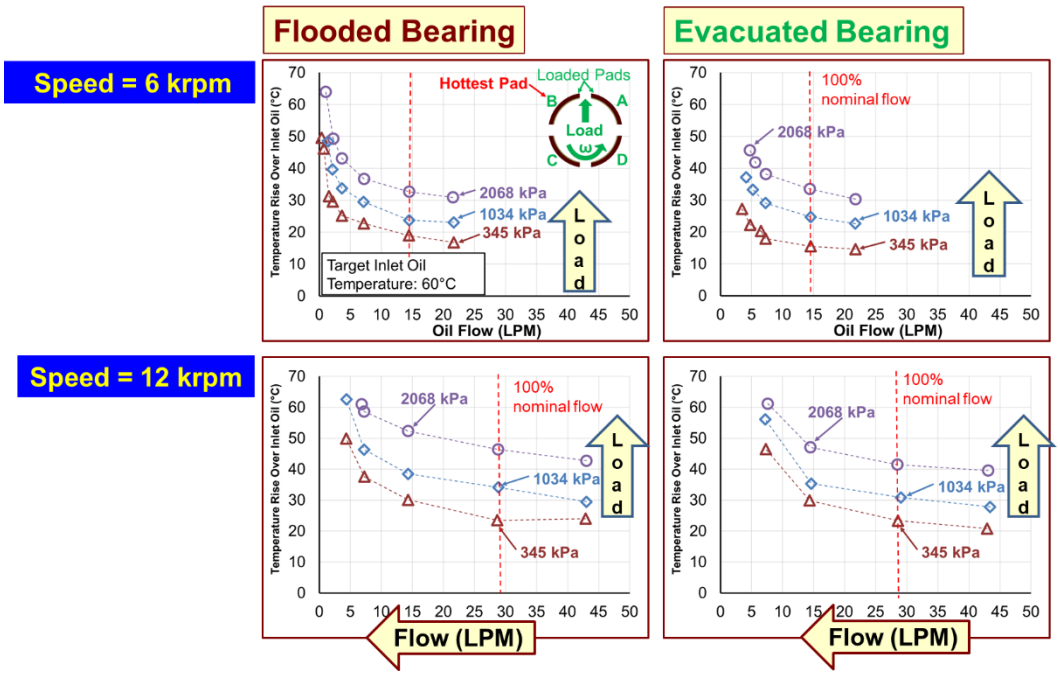

(a) Flooded bearing (orifice injection) **(b) Evacuated bearing** (spray bar injection)

Figure 7: Loaded pad highest temperature rise vs. flow rate (*Q*) for flooded bearing (left) **and evacuated bearing** (right)**. Operation with shaft speed = 6 krpm** (top graphs) **and 12 krpm** (bottom graphs)**, and three specific loads, W/(*LD*)=345 kPa, 1,034 kPa, and 2,068 kPa.** Oil inlet temperature = 60ºC.

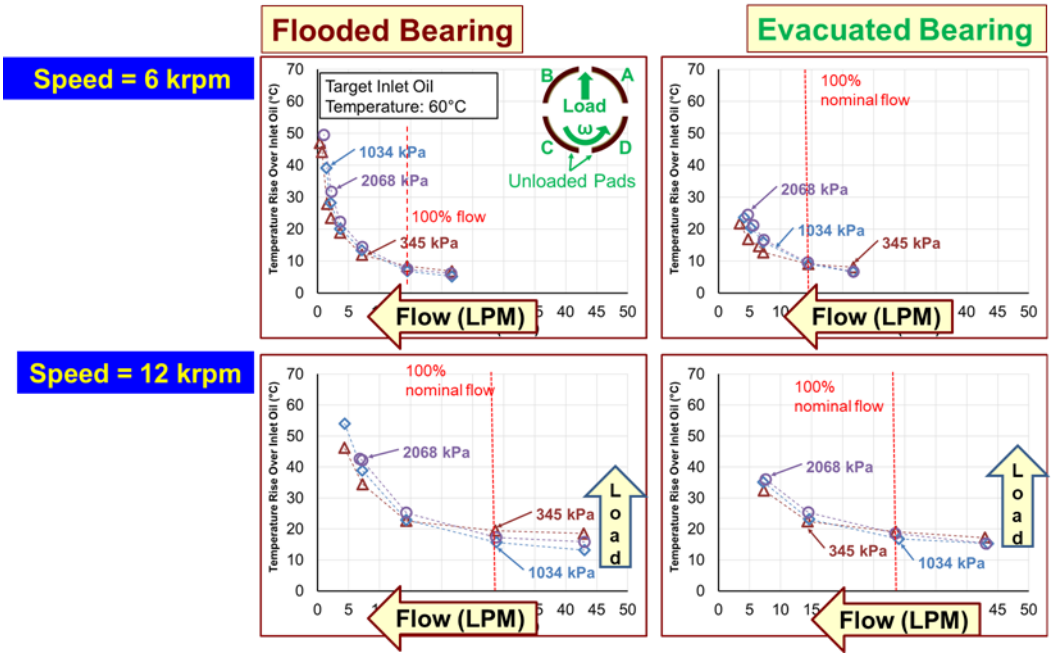

(a) Flooded bearing (orifice injection) **(b) Evacuated bearing** (spray bar injection)

Figure 8: Unloaded pad temperature rise vs. flow rate (*Q*) for flooded bearing (left) **and evacuated bearing** (right)**. Operation with shaft speed = 6 krpm** (top graphs) **and 12 krpm** (bottom graphs)**, and three specific loads, W/(*LD*)=345 kPa, 1,034 kPa, and 2,068 kPa.** Oil inlet temperature = 60ºC.

Toner [9] also shows measurements of the static pressure in the feed groove and which amount to a fraction of one bar for the lowest flow condition. On the other hand, to supply the nominal flow rate (100%), the oil static pressure drop (ΔP) equals 45 kPa (6.5 psig) at 6 krpm, and 91 kPa (13.0 psig) at 12 krpm. In general, $Q \sim \Delta P^{1/2}$

Lubricant exit temperature

The lubricant exit temperature (T_{out}) is recorded on the sides of the bearing, after the end seals (or pad retainers) and before the oil return drains. Figure 9 presents the oil exit temperature rise ($\Delta T = T_{out} - T_{in}$) vs. flowrate for the flooded bearing (left graphs) and the evacuated bearing (right graphs) and operation with shaft speed = 6 krpm (top graphs) and 12 krpm (bottom graphs). Incidentally, the results for the evacuated bearing are lesser in number than those for the flooded bearing. It is worthy of note that (some of) the thermocouples recording the oil exit temperatures did not work well during a few tests. The said data is not included in the Figure.

In general, the oil exit temperature increases with a reduction in flow as well as with an increase in shaft speed. As expected, the lubricant exiting the flooded bearing reached a higher temperature than that for the evacuated bearing. The applied load does not produce significant changes in lubricant exit temperature. Note that for the flooded bearing, for low flow rates $Q < 5$ LPM, the oil exit temperature rise is rather high; it reaches a magnitude above 40ºC for operation at 12 krpm shaft speed. On the other hand, measurements of the oil exit temperature for the evacuated bearing conducted at 6 krpm and a low load (0.345 MPa) appear rather low (nearly 0ºC); hence not believable.

Note the recorded oil exit temperatures are not representative of the temperatures recorded in the bearing pads (shown in Figs. 7 and 8), in particular for the flooded bearing supplied with a trickle of (nominal) flow.

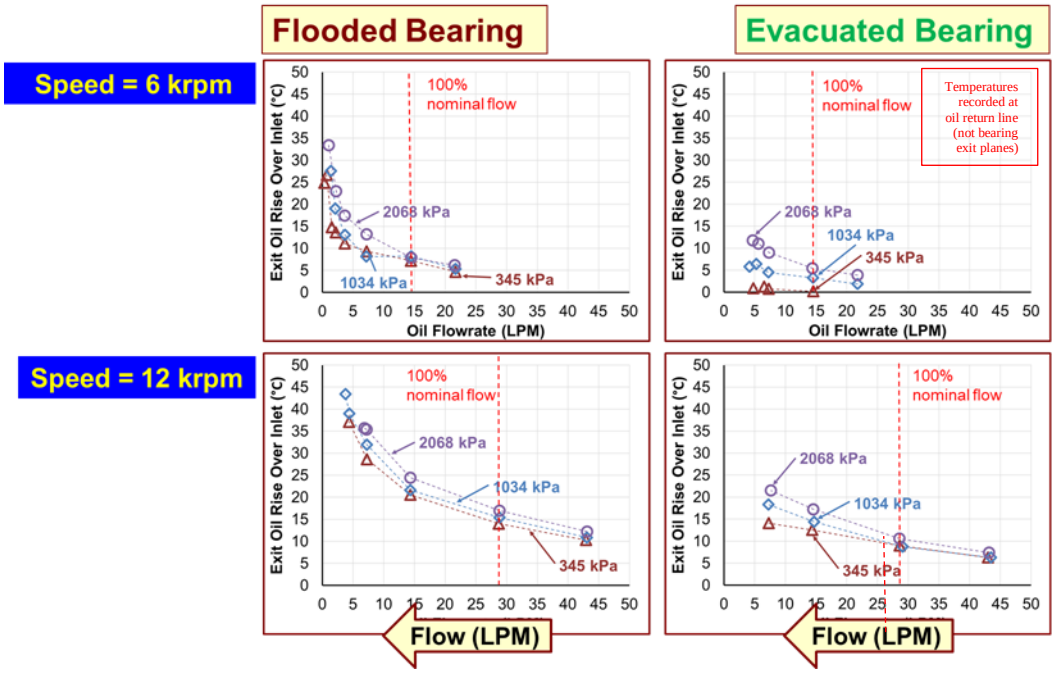

(a) Flooded bearing (orifice injection) **(b) Evacuated bearing** (spray bar injection)

Figure 9: Oil exit temperature rise vs. flow rate for flooded bearing (left) **and evacuated bearing** (right). **Operation with shaft speed = 6 krpm [32 m/s]** (top graphs) **and 12 krpm [64 m/s] and three specific loads, W/(*LD*)=345 kPa, 1,034 kPa, and 2.068 kPa.** Temperature rise relative to oil inlet temperature T_{in} = 60ºC.

Estimated drag power loss based on heat flow carried by lubricant

The test rig has a strain gauge type (wireless) torque meter that directly measures the drive torque (T_o). The drag power loss $P_o = (T_o \times \Omega)$. Refs. [8,9] present the measured drag torque and the calculated power loss (P_o) obtained for the flooded bearing. Unfortunately, the torque meter was not operational during the experiments with the evacuated bearing.

An estimation of the bearing drag power loss (P_{est}) follows from the heat carried away by the lubricant flowrate (Q), i.e.

$$\rho\, c_P\, Q\, (T_{out} - T_{in}) \rightarrow \kappa P_{est} \tag{6}$$

where ρ and c_P are the lubricant density and specific heat, and κ is an empirical parameter denoting the fraction of drag power advected as heat by the lubricant flow. Presently $\kappa \sim 0.95$ is used for Eq. (6) to predict a drag power just 5% away from the measured[3] drag power loss at 6 krpm and a low specific load (0.345 MPa) obtained with the flooded bearing.

Presently, the selection of $\kappa \sim 0.95$ obeys to the availability of the direct torque measurement that permits its empirical quantification. As the review of past literature argues, the estimated power losses derived from the supplied flow and the oil exit temperature raise; i.e. $P_{est} \sim Q\,\Delta T$, does not always concur with a direct measurement of the drag torque times the shaft angular speed.

Figure 10 depicts the estimated drag power (P_{est}) vs. flowrate for operation at two shaft surface speeds and under three specific loads. Recall Fig. 9 shows the oil exit temperature difference $(T_{out} - T_{in})$. Below the nominal flow condition (100% flow), P_{est} is proportional to the supplied flow (Q), whereas for larger flow rates, P_{est} is a little larger than that for the nominal flow. In general, the drag power for the evacuated bearing is significantly lower than that for the flooded bearing, in particular for operation at 12 krpm shaft speed. The difference amounts to 50% for the over flooded condition (150% flow).

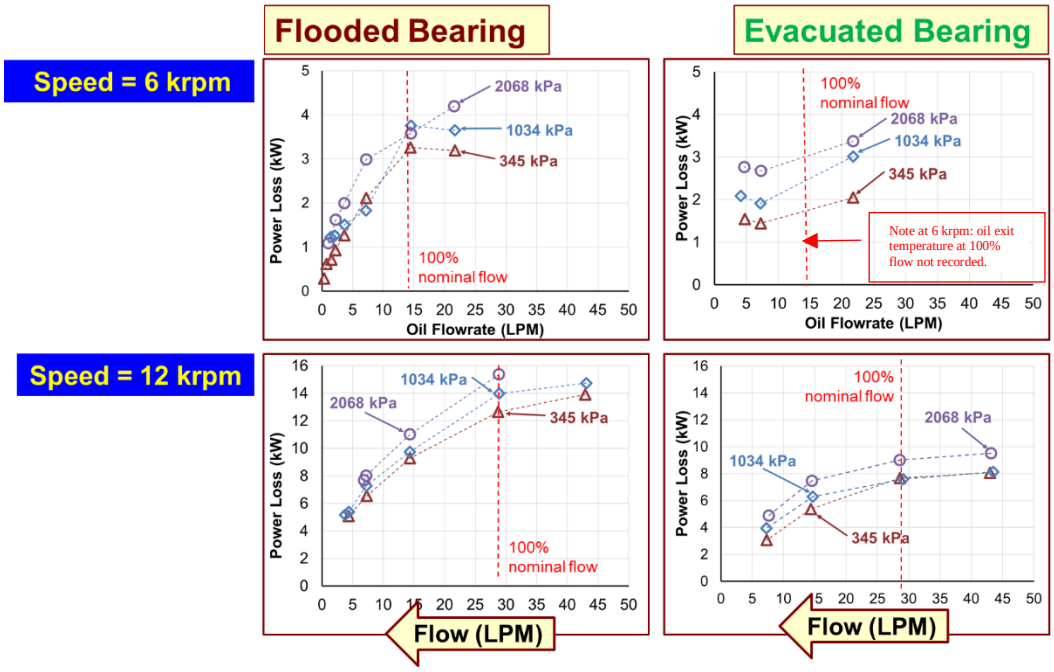

(a) Flooded bearing (orifice injection) **(b) Evacuated bearing** (spray bar injection)

Figure 10: Estimated power loss vs. flow rate (*Q*) for flooded bearing (left) **and evacuated bearing** (right). **Operation with shaft speed = 6 krpm** (top graphs) **and 12 krpm** (bottom graphs).

Experimental complex dynamic stiffnesses for test bearings

Figure 11 presents the real part of the complex stiffnesses H_{xx} and H_{yy} vs. frequency for the flooded bearing (top graphs) and the evacuated bearing (bottom graphs) for operation with shaft speed = 6 krpm and under two applied loads. Each graph shows the physical parameter for four magnitudes of supplied flow rate; 150%, 100% or nominal, 50% and 30% (or lower). Figure 12 depicts Re(H_{xx}) and Re(H_{yy}) for operation with shaft speed = 12 krpm.

In general, one can assess that Re(H_{yy}) > Re(H_{xx}), with both parameters increasing with the applied load. Shaft speed has little effect on the dynamic stiffnesses. Note Re(H_{yy}) and Re(H_{xx}) for the flooded bearing are slightly larger in magnitude than the corresponding parameters for the evacuated bearing. Importantly enough, for most cases, Re(H_{yy}) and Re(H_{xx}) do not show major variations with frequency ($\omega < 200$ Hz) and which make evident the fit Re(H)→K, and thus a small or null virtual mass coefficient, i.e. M=0. Moreover, note that for the lowest flow rates (and low load), the data for the evacuated bearing shows a pronounced scattering; likely due to the ease of oil evacuation as there is but a small volume of oil between the pads and the rotor. For the same operating conditions, Fig. 13 presents the imaginary part of H_{xx} and H_{yy}, respectively, vs. frequency and operation with shaft speed at 6 krpm. Figure 14 shows Im(H_{xx}) and Im(H_{yy}) for operation at 12 krpm.

[3] Recorded with a torque meter, see Ref. [7].

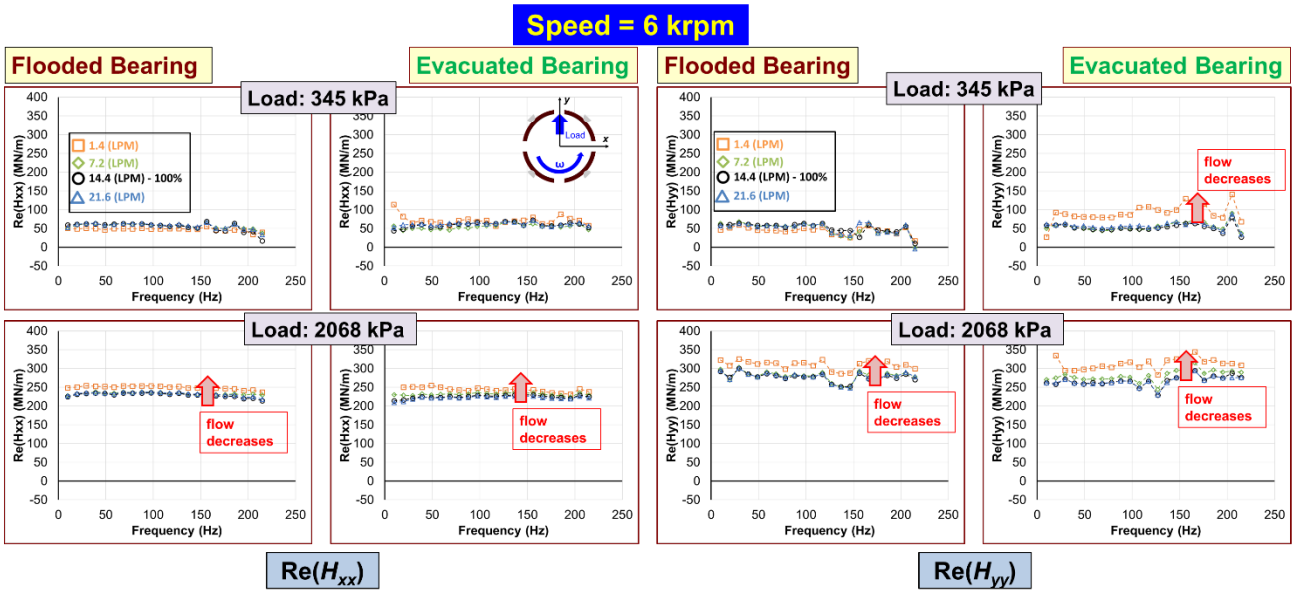

Figure 11: Real part of complex stiffnesses H_{xx} and H_{yy} for flooded bearing (single orifice injection**) and evacuated bearing (**spray bar injection**) vs. excitation frequency and for four flow rates. Operation at surface speed = 32 m/s (6 krpm) and two specific loads $W/(LD)$ = 345 kPa (**top graphs**) and 2,068 kPa (**bottom graphs**).**

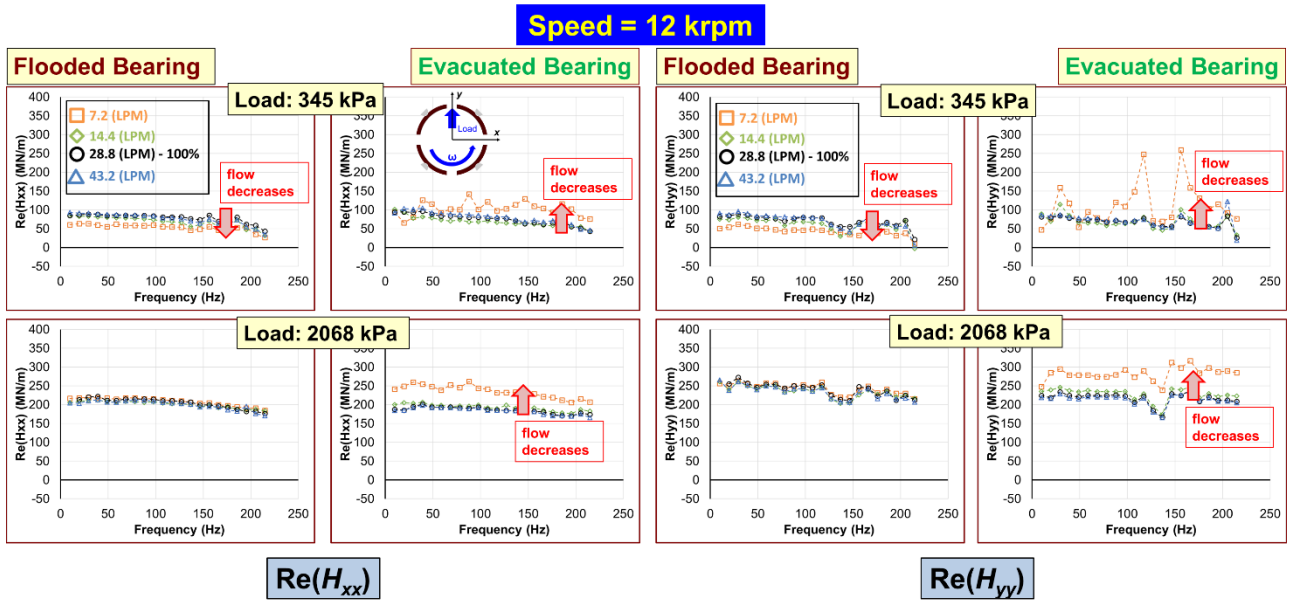

Figure 12. Real part of complex stiffnesses H_{xx} and H_{yy} for flooded bearing (single orifice injection**) and evacuated bearing (**spray bar injection**) vs. excitation frequency and for four flow rates. Operation at surface speed = 64 m/s (12 krpm) and two specific loads $W/(LD)$ = 345 kPa (**top graphs**) and 2,068 kPa (**bottom graphs**).**

In Figures 13 and 14, note that for most operating conditions, Im(H) is proportional to frequency (ω) thus showcasing its viscous character. For both flooded ends and evacuated ends bearings, as the flow rate decreases, so does Im(H). The obvious exception is for the evacuated ends bearing supplied with the smallest flow rate (30% or less of nominal) that produces unusual results as either Im(H_{yy}) and Im(H_{xx}) > 0 or < 0. For this particular bearing configuration supplied with a low flow rate, the profuse scatter in the data makes suspicious any estimation of a distinct damping coefficient from the fit Im(H) → ($C\omega$). In other words, the test data does not fit the physical model.

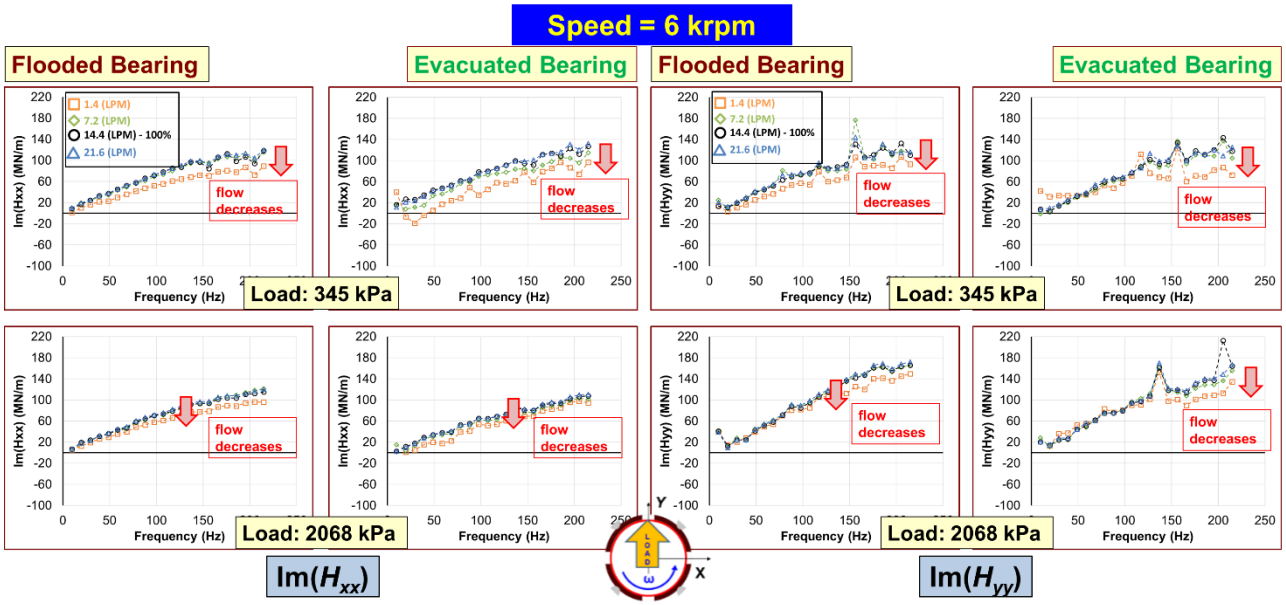

Figure 13: Imaginary part of complex stiffnesses H_{xx} and H_{yy} for flooded bearing (single orifice injection**) and evacuated bearing (**spray bar injection**) vs. excitation frequency and for four flow rates. Operation at surface speed = 32 m/s (6 krpm) and two specific loads *W/(LD)* = 345 kPa (**top graphs**) and 2,068 kPa (**bottom graphs**).**

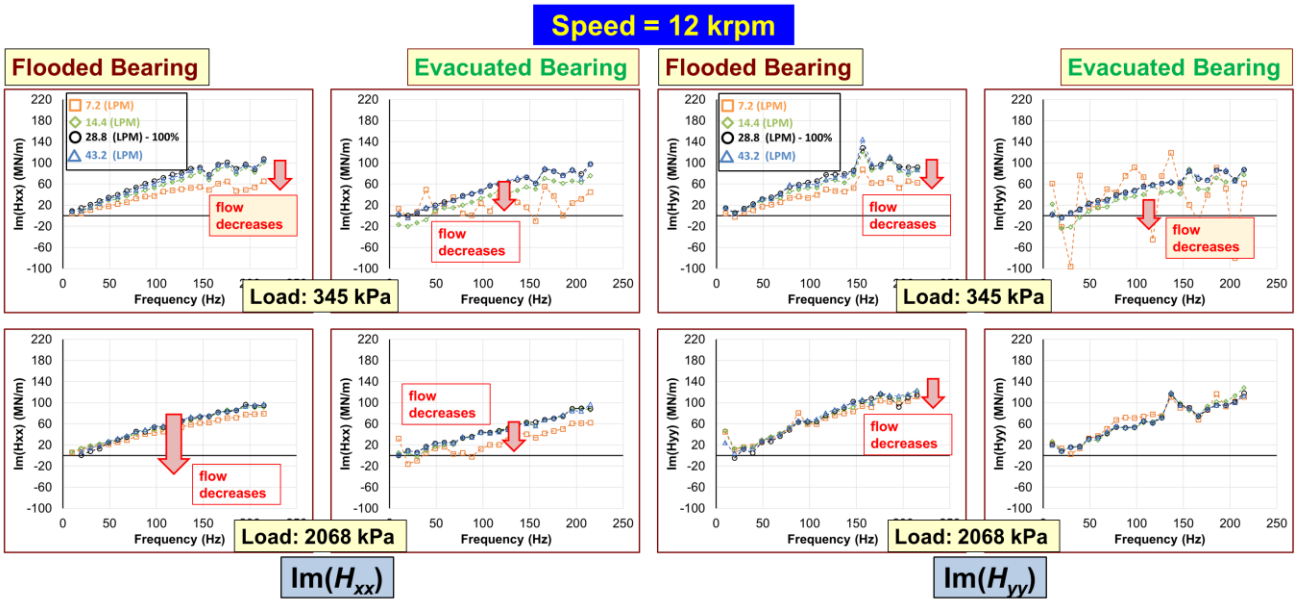

Figure 14: Imaginary part of stiffnesses H_{xx} and H_{yy} for flooded bearing (single orifice injection**) and evacuated bearing (**spray bar injection**) vs. excitation frequency and for four flow rates. Operation at surface speed = 64 m/s (12 krpm) and two specific loads *W/(LD)* = 345 kPa (**top graphs**) and 2,068 kPa (**bottom graphs**).**

Identified stiffness and damping coefficients for test bearings

The bearing stiffness (K) and virtual mass (M) coefficients follow from a simple curve fit, Re(H) → (K-$M\omega^2$) over a frequency range that includes the synchronous shaft frequency. Similarly, Im(H) → ($C\omega$) delivers the damping coefficient (C).

For both bearings, one with flooded and with single orifice injection, and the other evacuated and with oil spray bars, Figure 15 depicts the direct stiffnesses (K_{xx}, K_{yy}) vs. supplied flow rate for operation with shaft speeds = 6 krpm and 12 krpm and under three applied loads. Similarly, Figure 16 shows the identified direct damping coefficients (C_{xx}, C_{yy}) for the same flow and operating conditions.

Note that cross-coupled force coefficients, (K_{xy}, K_{yx}) and (C_{xy}, C_{yx}), are small in magnitude when compared to the direct force coefficients, thus not shown here. Recall in Fig. 6 that the attitude angle is sizeable for low loads and low flow conditions. In general,

for moderate to large loads (>1,034 kPa), the parameter identification process produces minute cross-coupled stiffnesses, a small fraction of the direct ones. On the other hand, for the low load (345 kPa), K_{xy} and K_{yx} can be as large as 40% of the direct stiffness. For more details, please see Appendix B in the thesis of Toner [9].

In general, for the flooded bearing, $K_{yy} \sim K_{xx}$ for the lowest and intermediate loads, whereas $K_{yy} > K_{xx}$ for the largest applied unit load. Shaft speeds seem to have a minor effect on both K_{yy} and K_{xx}, although high speed produces lower stiffness magnitudes for both flooded and evacuated bearings. Similarly, oil flowrate varying from 150% to 25% of the nominal conditions has a minor effect on the bearing direct stiffnesses.

In general, the evacuated bearing show stiffnesses with a lower magnitude as the corresponding ones for the flooded bearing; the difference amounts to ~ 20%. However, for the low flow condition, the stiffnesses for the evacuated bearing show a more rapid growth. In particular for operation at 12 krpm and for the intermediate unit load (1,034 kPa), note K_{xx} and K_{yy} are larger in magnitude than the stiffnesses obtained for a load of 2,068 kPa.

As per the damping coefficients for the flooded bearing operating at 12 krpm, both $C_{xx} \sim C_{yy}$ are significantly smaller in magnitude than the coefficients obtained at shaft speed = 6 krpm; see Fig. 16. The applied load has a rather small effect on the damping coefficients for operation at 12 krpm. Not so for tests with shaft speed = 6 krpm that produce $C_{xx} < C_{yy}$, in particular for the highest load.

The supplied flow rate has no effect on the damping coefficients for flow rates as low as 25% of nominal. A further reduction to a very small flow rate, as obtained from experiments at 6 krpm and 12 krpm, does produce a drop in direct damping coefficients, about a 20% or so reduction when compared to the coefficients obtained at the nominal flow condition.

For the evacuated bearing, $C_{xx} \sim C_{yy}$ for the data collected with shaft operation at 12 krpm. Experimental results at 6 krpm, on the other hand, show $C_{xx} < C_{yy}$, in particular for unit load = 1,034 kPa and higher. Note also that as the flow rate decreases well below nominal, C_{yy} at 6 krpm quickly decreases for the three applied loads. At a shaft speed of 12 krpm, for the lowest flow condition (25% nominal), C_{xx} drops rapidly whereas C_{yy} increases for two of the three loads shown. This is a striking difference when comparing to C_{yy} for the flooded bearing and which shows a consistent reduction in damping magnitude.

Recall that the damping coefficients herein shown are representative of dynamic load excitations with frequencies well within the range used for the curve fit, typical up to 250 Hz. Importantly enough, the damping coefficients presented in the figures should not be used for rotor excitation frequencies $\omega > \Omega$ (1X), in particular for operation at 12 krpm (200 Hz). Figures 13 and 14 provides rationale for the assertion since at large frequencies, $\omega > \Omega$, neither Im(H_{xx}) nor Im(H_{yy}) appear to proportionally grow with frequency (ω).

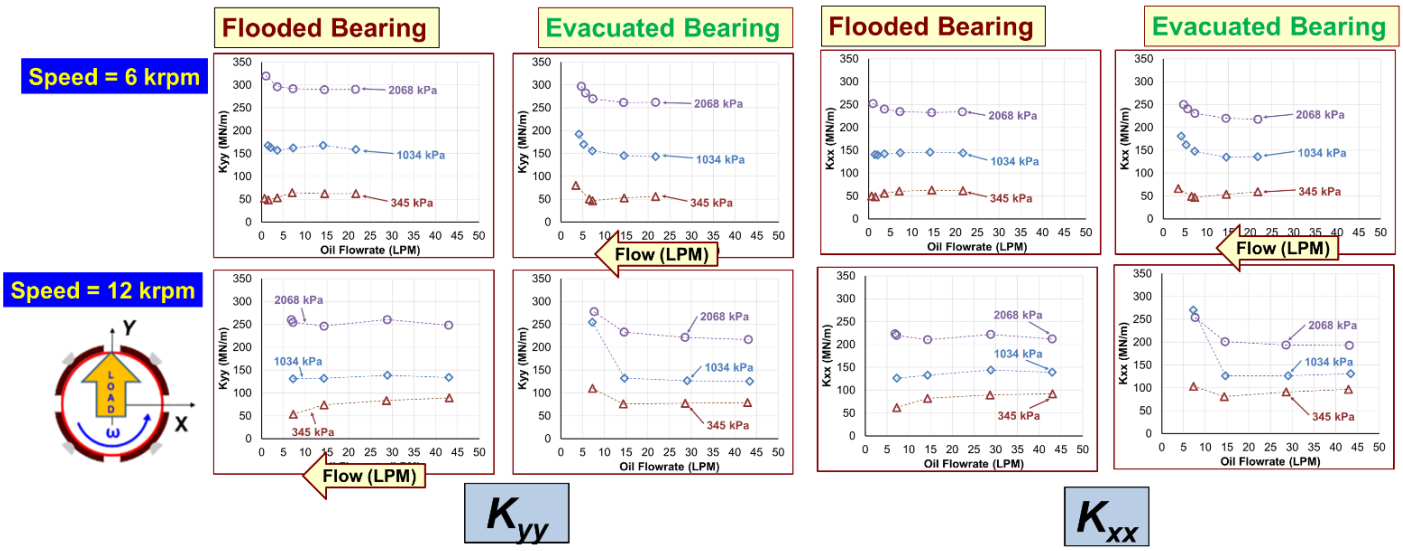

Figure 15: Bearing stiffnesses K_{yy} and K_{xx} vs. flow rate (Q) for flooded bearing (single orifice injection**) and evacuated bearing (**spray bar injection**). Operation with shaft speed = 6 krpm** (top graphs) **and 12 krpm** (bottom graphs).

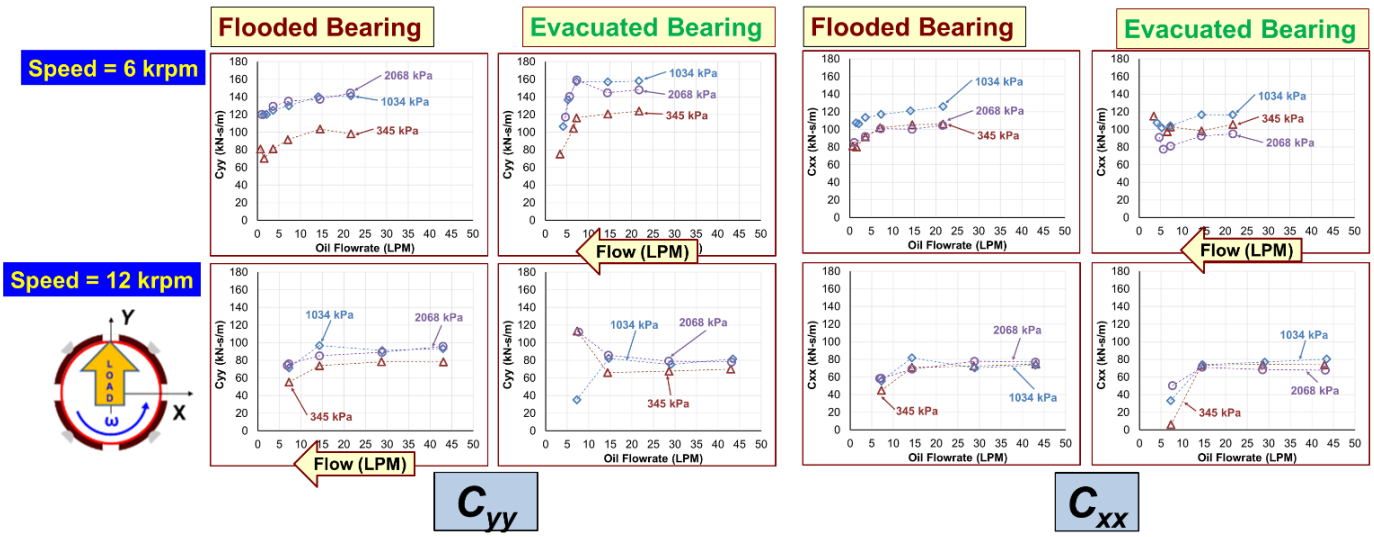

Figure 16: Bearing damping coefficients C_{yy} and C_{XX} vs. flow rate (Q) for flooded bearing (single orifice injection**) and evacuated bearing (**spray bar injection**). Operation with shaft speed = 6 krpm** (top graphs) **and 12 krpm** (bottom graphs).

For completeness, Figure 17 shows the virtual mass coefficient (M_{yy}) vs. supplied flow rate for operation with shaft speed = 6 krpm. The coefficient $M_{xx} \sim 0$, and not shown for brevity. The flooded bearing produces $M_{yy} > 0$, whereas the evacuated bearing evidences $M_{yy} < 0$. In spite of the differences, both in sign and in apparent magnitude, $|M_{yy}| \sim 10$ kg to 20 kg, the effect of the virtual mass to the dynamic stiffness ($K_{yy} - \omega^2 M_{yy}$) is rather small, as easily seen in Figures 11 and 12 that portray a fairly flat Re(H_{yy}) as the excitation frequency (ω) increases.

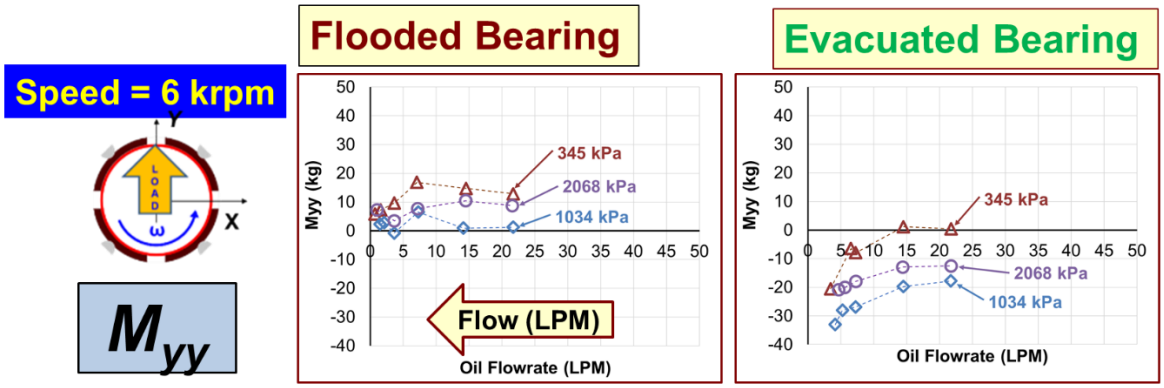

(a) Flooded bearing (orifice injection) **(b) Evacuated bearing** (spray bar injection)

Figure 17: Virtual mass coefficient M_{yy} (along load direction) vs. flow rate (Q) for flooded bearing (single orifice injection**) and evacuated bearing (**spray bar injection**). Operation with shaft speed = 6 krpm.**

Subsynchronous whirl motions in bearing supplied with a low flow rate

Reporting in full the experimental results for the flooded bearing, Refs. [8,9] describe the appearance of subsynchronous shaft vibrations (SSV) [1] for operating conditions under a low specific load (345 kPa at 6 krpm) and with the bearing supplied with low magnitudes flow rates, 15% → 2% of nominal. The found SSV "hash" has a broad band frequency spectrum well below the synchronous frequency and lacking discrete frequency peaks; however the amplitude of the SSV is rather small compared to the bearing synchronous motion amplitude.

Similar measurements conducted with the evacuated bearing were less concerted; albeit SSV did happen but at a flow rate larger than that for the flooded bearing. Figure 18 depicts the said measurements to demonstrate SSV hash is more severe for conditions with low flow and a low applied load.

Recall the bearing performance is a function of the shaft speed, applied load and supplied flow; all controlled parameters. Under no condition the test bearing operation, flooded or evacuated, appeared compromised due to the presence of the rather incipient SSV hash.

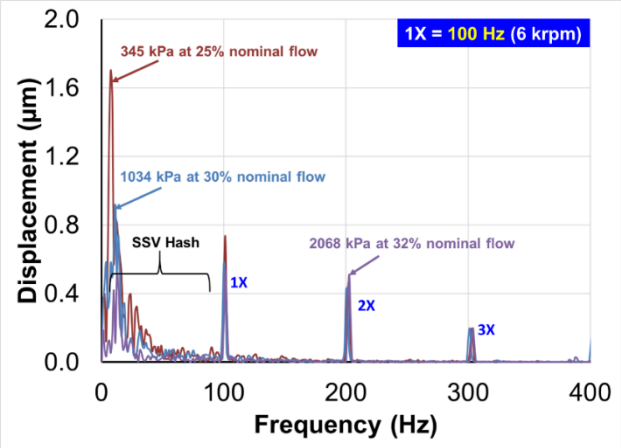

Figure 18: Evidence of SSV hash in evacuated bearing with spray bar injection: amplitude of shaft motion vs. frequency. Shaft speed = 6 krpm and operation at various loads and with flow rate at 25% - 32% of nominal flow rate (=14.4 LPM).

CONCLUSION

Machine efficiency improves as the power losses in bearings reduce, hence an operation mode that reduces the supplied flow brings immediate benefits. Bearing procurement that calls for reduced lubricant flow also decreases capital expenditures along with equipment footprint, i.e. smaller size pumps and oil reservoirs. However, the efficiency improvement must preserve the mechanical element robustness while maintaining pad metal temperatures low enough for long-term operation (< 130°C) [7].

The lecture herein quantifies the effect of lubricant flowrate on the performance of a flooded bearing against that of an evacuated bearing. The test TPJB has four-pads with center pivots, diameter D=102 mm and length L=0.6 D. The flooded bearing is supplied with lubricant through single orifices whereas the evacuated bearing has spray bars. The experiments include operation at two shaft speeds = 6 krpm and 12 krpm (= 64 m/s surface speed) and under three applied specific loads = 0.345 MPa, 1.03 MPa and 2.07 MPa in a load-between pad (LBP) configuration. The lubricant is ISO VG 46 oil supplied at 60°C, and the flowrate supplied ranged from 150% to ~25% (or lesser) of a nominal magnitude that is proportional to shaft speed. That is, the flow rate at the high shaft speed (12 krpm) is twice that for the low shaft speed at 6 krpm.

Derived from the experimental results for both TPJB constructs, the learning is:

- Both bearing configurations operate with shaft eccentricities increasing with applied load and decreasing with shaft speed. A reduction in flow rate makes the bearing more eccentric. In particular, the evacuated bearing shows a large eccentricity not often aligned (or parallel) to the applied load, i.e., a sizeable attitude angle. Some measurements at the lowest applied load and with just ~25% of nominal flow produced a significant increase in static eccentricity.
- The evacuated bearing with spray bar injection has its loaded pad at a lower temperature (a few °C below) than the same pad temperature for the flooded bearing with single orifice injection. Similarly, the oil exit temperature is lower, in particular for an over flooded condition, i.e. flow rate 50% above nominal.
- An estimated drag power losses derived from the supplied flow and exit oil temperature rise shows the evacuated bearing produces up to ~ 40% lesser power loss than the flooded bearing. The most significant difference occurs for operation with flow rates 50% larger than the nominal flow.
- The bearings direct stiffnesses K_{xx} and K_{yy} increase with the applied load and show little dependency on shaft speed. The evacuated bearing produces (up to) ~ 20% lesser magnitude stiffnesses than the flooded bearing. Note that both bearing configurations show dynamic direct stiffnesses not varying with frequency; hence, the estimated virtual masses (M) are relatively unimportant.
- Damping coefficients C_{xx} ~ C_{yy} do vary with the supplied flowrate. With the flooded bearing and for operation at 6 krpm, C's decrease up to 28% as the flow rate decreases from 150% to just a few % of nominal flow. A similar behavior is attained for operation with shaft speed = 12 krpm, though with a larger drop (35% or so) as the flow decreases. The evacuated bearing produces lesser damping coefficients than the flooded bearing. For the lowest flowrate (25% of nominal) considered, the estimated damping coefficients are highly uncertain.
- During experiments with the lowest load (0.345 MPa) and at a shaft speed=6 krpm, the bearing motion showed a broadband subsynchronous vibration (SSV) when supplied with a very low flowrate, ~25% of nominal for the evacuated bearing and 2%-15%

for the flooded bearing. The amplitude of motion was rather small and did not impair the operation of the test bearings, flooded or evacuated.

The experimental campaign demonstrates that tilting pad bearings (flooded and evacuated) can safely operate with a reduced flow rate (50% or so of nominal) to produce significant savings in drag power losses and with no significant effect on the pads' metal temperatures. In addition, the reduction in flow to ½ the nominal condition does not greatly affect the bearing force coefficients. A major concern related to loss of damping under low flow conditions became apparent only when supplying the bearing with minute fractions of the supplied flow, i.e. a severe staved flow condition.

ACKNOWLEDGMENTS

Thanks to the TAMU Turbomachinery Research Consortium (TRC) for the financial support that enabled the education of graduate students. TRC funds include payment of a monthly salary, fringe benefits and educational tuition and fees.

Thanks to Mr. Jon Toner, graduate research assistant, for conducting the measurements and for training Mr. Alcantar on the operation and troubleshooting of the test rig and its components. The authors are solely responsible for the technical content and discussion.

Thanks to Mr. John Whalen, TAC Emeritus member, for leading the review process and for providing incisive comments and recommendations that greatly improved the quality of the final manuscript.

The first author dedicates this paper to the memory of Mr. Scan DeCamillo, a formidable engineer and a true friend of the laboratory. The whole turbomachinery community will miss Scan for a long time. He is gone to rock in another world.

NOMENCLATURE

C_r	Bearing radial clearance [m]
$C_{\alpha\beta}$	Bearing damping coefficients, $\alpha,\beta = x,y$ [Ns/m]
c_P	Lubricant specific heat [J/(kg ^{o}C)]
D	Shaft diameter [m]
e	Bearing eccentricity [m]
$H_{\alpha\beta}$	Bearing complex dynamic stiffness coefficients, $\alpha,\beta = x,y$ [N/m]
$K_{\alpha\beta}$	Bearing stiffness coefficients, $\alpha,\beta = x,y$ [N/m]
K_S	Bearing support rods stiffness [N/m]
L	Bearing length [m]
$M_{\alpha\beta}$	Bearing virtual mass coefficients, $\alpha,\beta = x,y$ [N/m]
M_H	Bearing housing and assembly mass [kg]
N_p	Number of pads in bearing
P_o	$(T_o\ \Omega)$. Bearing drag power loss [W]
P_{est}	Estimated drag power loss [W]
Q	Oil supply flow rate [m^3/s]
T_o	Drag torque [Nm]
T	Temperature [^{o}C]
T_{in}, T_{out}	Oil inlet and exit temperatures [^{o}C]
W	Applied static load (along Y) [N]
λ	Fraction of lubricant from upstream pad carried to downstream pad
κ	Fraction of drag power loss carried by lubricant flow
ρ, μ	Oil density [kg/m^3] and viscosity [Pa.s]
Ω	Rotor angular speed [rad/s]
ω	Excitation frequency [rad/s]

Vectors and matrices

a	$[a_x, a_y]^T$ **.** Acceleration of bearing [m/s^2]
F	$[F_x, F_y]^T$ **.** Vector of applied forces [N]
$\mathbf{F_B}$	Vector of fluid film bearing reaction forces [N]
$\mathbf{F_S}$	Vector of bearing housing support reaction forces [N]
H	$[H_{xx}, H_{xy} \mid H_{yx}, H_{yy}]$**.** Matrix of complex dynamic stiffnesses [N/m]
x	$[d_x, d_y]^T$ **.** Displacement of bearing relative to shaft [m]

Abbreviations

LBP	Load between pads
SSV	Subsynchronous vibration

TBJB Tilting pad journal bearing
1X ω=Ω. Synchronous frequency. 2X: ω=2 Ω

REFERENCES

[1] DeCamillo, S., He, M., Cloud, C. H., and Byrne, J., 2008, "Journal Bearing Vibration and SSV Hash," Proceedings of the 37th Turbomachinery Symposium, The Turbomachinery Laboratory, Texas A&M University, September 7-11, Houston, TX, USA, pp. 179-194, https://doi.org/10.21423/R1DH1J.

[2] Leopard, A. J., 1976, "Tilting Pad Bearings-Limits of Operation," ASLE Lubrication Engineering, 32(2), pp. 637-644.

[3] Dmochowski, W. M., and Blair, B., 2006, "Effect of Oil Evacuation on the Static and Dynamic Properties of Tilting Pad Journal Bearings," Trib. Trans., **49**, pp. 536-544. https://doi.org/10.1080/10402000600885175.

[4] Coghlan, D., 2014, "Static, Rotordynamic, and Thermal Characteristics of a Four Pad Spherical-Seat Tilting Pad Journal Bearing with Four Methods of Directed Lubrication," M. S. Thesis, Texas A&M University, College Station, Texas.

[5] San Andrés, L., and Abdollahi, B., 2018, "Improved Estimation of Bearing Pads' Inlet Temperature: A Model for Lubricant Mixing at Oil Feed Ports and Validation against Test Data," II Asia Turbomachinery and Pump Symposium, The Turbomachinery Laboratory, Texas A&M University, Mar. 13–15, Singapore, https://oaktrust.library.tamu.edu/handle/1969.1/172520.

[6] San Andrés, L., Jani, H., Kaizar, H., and Thorat, M., 2020, "On the Effect of Supplied Flow Rate to the Performance of a Tilting-Pad Journal Bearing. - Static Load and Dynamic Force Measurements," ASME J Gas Turbines Power, **142**(2), pp. 121006, https://doi.org/10.1115/1.4048798

[7] Jani, H., 2018, "Measurements of the Static and Dynamic Force Performance on a Five-Pad, Spherical-Pivot Tilting-Pad Journal Bearing: Influence of Oil Flow Rate," M.S. Thesis, Texas A&M University, College Station, TX, USA.

[8] San Andrés, L., Toner, J., and Alcantar, A., 2021, "Measurements to Quantify the Effect of a Reduced Flow Rate on the Performance of a Tilting Pad Journal Bearing (LBP) with Flooded Ends," ASME J. Eng. Gas Turbines Power, Vol. **143**(11): 111012, https://doi.org/10.1115/1.4052268

[9] Toner, J., 2020, "Measurements of the Static and Dynamic Force Performance on a Five-Pad, Spherical-Pivot Tilting-Pad Journal Bearing: Influence of Oil Flow Rate," M.S. Thesis, Texas A&M University, College Station, TX, USA.

[10] DeCamillo, S. and Brockwell, K., 2001, "A Study of Parameters that Affect Pivoted Shoe Journal Bearing Performance in High-Speed Turbomachinery", Proceedings of the 30th Turbomachinery Symposium, The Turbomachinery Laboratory, Texas A&M University, September 17-20, Houston, TX, USA, pp. 9-22, https://doi.org/10.21423/R1PW8G

[11] Nicholas, J.C., Elliott, G., Shoup, T., amd E., Martin, 2008, "Tilting Pad Journal Bearing Starvation Effects", Proceedings of the 37th Turbomachinery Symposium, The Turbomachinery Laboratory, Texas A&M University, September, Houston, TX, USA, https://doi.org/10.21423/R1TS8P

[12] Whalen, J. K., He, M., Cerny, V., and Polreich, V., 2015, "The Effects of Starvation on the Dynamic Properties of Tilting Pad Journal Bearings," Proc. 44th Turbomachinery Symposium, The Turbomachinery Laboratory, Texas A&M University, September 14-17, Houston, TX, USA, pp. 1-10, https://doi.org/10.21423/R13922

[13] Childs, D. W., Rodriguez, L., Cullota V., Al-Ghasem, M. and Graviss, M., 2006, "Rotordynamic-Coefficients and Static (Equilibrium Loci and Leakage) Characteristics for Short, Laminar-Flow Annular Seals," ASME J. *Tribol*, **128**(2), pp. 378-387. https://doi.org/10.1115/1.2164468.

[14] San Andrés, L., 2009, "Experimental Identification of Bearing Force Coefficients," *Modern Lubrication Theory*, Notes 14, Libraries Texas A&M University Repository, http://oaktrust.library.tamu.edu/handle/1969.1/93197 [access date June 10, 2020].

